Feature width miniaturization in atom nanolithography with double standing wave layers

Pingping Zhang (张萍萍)*, Yan Ma (马 艳), and Tongbao Li (李同保)

Department of Physics, Tongji University, Shanghai 200092, China

**Corresponding author: zpp_789@163.com*

Received April 3, 2012; accepted June 26, 2012; posted online October 26, 2012

Periodic nanostructures spaced by half of the wavelength can be obtained by the technology of laser-focused atomic deposition. Experimental result with single standing wave layer is presented, with a periodicity of 213 ± 0.1 nm, a height of 4 nm, and a feature width of 64 ± 6 nm. To further minimize the feature width,focusing and depositing characteristics of double standing wave layers are numerically simulated with optimized particle optics model. It is shown that the spherical aberration is reduced significantly. The predicted feature width is 18.2 nm and the height is approximately 12.6 nm when the powers of the two standing wave layers are 6 and 14 mW, respectively. Well-defined line occurs even when the full-width at half-maximum (FWHM) of transverse angular spread reaches 0.5 mrad.

OCIS codes: 140.3325, 220.3740, 220.4241.

doi: 10.3788/COL201210.S21403.

The fabrication of nanoscale structures by neutral atom lithography has the potential to significantly put forward the nanotechnology, ranging from device miniaturization in electronic industry to nanometrology. Over the last two decades, one-dimensional (1D) structures with this direct deposition technique have been grown with sodium[1], chromium[2,3], cesium[4,5], aluminum[6], ytterbium[7], iron[8], barium[9], and metastable helium[10]. Focusing and depositing characteristics of single standing wave layer (SL) with particle optics model have been studied in great detail by McClelland *et al.*[11−15]. The standing wave light field acts as an array of cylindrical lenses for the incident atomic beam analogous to conventional optics lens, focusing the atoms on the substrate. The standing wave microlens arrays are not perfect just like their conventional optical counterparts, for they suffer from multiple aberrations. Because of the nonparabolic nature of the light-induced potential, the focusing of atoms is subject to spherical aberrations giving a finite width to the deposited features as well as a more or less homogeneous background. Longitudinal velocity spread corresponds to chromatic aberrations and broadens the microlens focus as well. Transversal beam spread significantly broadens the spot size of the microlens focus, which can be controlled by laser cooling. The elimination of various aberrations in conventional optics can be realized by a combination of a set of lens. Similarly, a pair of light masks, made from double standing light wave layers (DL), may in principle reduce the focusing imperfections including spherical aberration and transverse angular divergence. Arun *et al.*[16] have done some pioneer work on this topic. However, most of their work focuses on the local optimization of the parameters. In this letter, experimental result with SL is presented firstly and in an effort to further minimize the feature width, studies concerning the properties of DL will be given with optimized particle optics model[15].

Atom lithography with SL which serves as a focusing mask, free from matter, for a suitable substrate is depicted in Fig. 1[5]. After travelling through small atomic lens arrays formed by a near-resonant standing wave, the light force exerted on an atom enables an atomic beam to concentrate exactly at the nodes (blue detuning) or the anti-nodes (red detuning) of the standing wave. When a silicon substrate is located sufficiently close and parallel to the light field, a series of well-defined periodic lines will be seen, spaced right half of the wavelength.

Figure 2 shows the atomic force microscope (AFM) image of the deposited sample with SL in our group[3]. The wavelength of the laser in vacuum is 425.55 nm with respect to ^{52}Cr atomic transition $^7S_3 \rightarrow {}^7P_4^0$. The $1/e^2$ radius of the Gaussian beam (w_0) is roughly 100 μm. The laser frequency for deposition is blue shifted 500×2π MHz by an acoustic optic modulator from the resonance. The total input power of the laser is 180 mW, including laser frequency stabilization of 24 mW, laser cooling of 31 mW, and laser focusing of 15 mW. To avoid the diffraction, the silicon substrate is separated from the center of the Gaussian beam by 1.5 w_0. After a deposition time of 62 min, the sample is taken out from the vacuum chamber and then examined by AFM. The AFM image of the sample shows the surface three-dimensional (3D) topography of a 5×5-μm area and a height of 4 nm. Periodic chromium lines with mean periodicity of 213 ± 0.1 nm is obtained, and the feature width presented is 64±6 (nm). Although the deposited lines of the nanograting are well-defined, the feature width is far from satisfactory.

The arrangement of DL is shown in Fig. 3. The intensity profile of light field is given by

$$I(x,z) = I_1 \exp\left(\frac{-2z^2}{w_1^2}\right)\sin^2(kx+\varphi) + I_2 \exp\left[\frac{-2(z-D)^2}{w_2^2}\right]\sin^2(kx), \quad (1)$$

where D is the separation between the two standing waves,w_1 and w_2 denote the $1/e^2$ radius of the two laser beams, respectively, and $k = 2\pi/\lambda$, where λ is the wavelength. $I_1 = 2P_1/\pi w_1^2$ and $I_2 = 2P_2/\pi w_2^2$ represent the peak intensities of the two standing waves, respectively,

 © 2012 Chinese Optics Letters

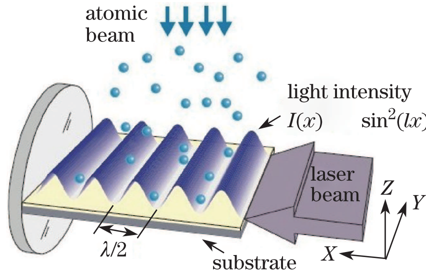

Fig. 1. Geometry for laser-focused atomic deposition.

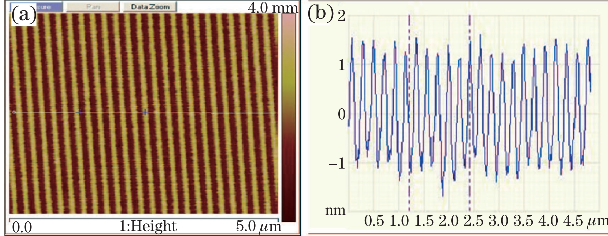

Fig. 2. (a) AFM image of Cr features with SL. The image covers an area of 5×5 (μm) . The periodicity of sample is 213±0.1 nm by power spectrum density (PSD) calculation; (b) line profile is shown by the section analysis, and the location analyzed is indicated on the AFM image with white bright line. Lines are approximately 64±6-nm wide and 4-nm high.

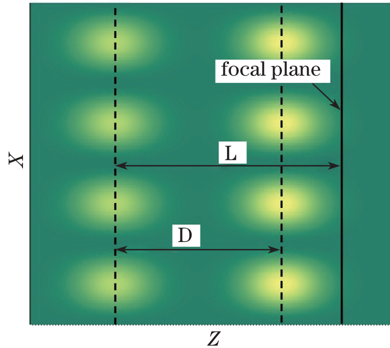

Fig. 3. Schematic of DL. The contour shows sinusoidal variation envelopes along the x axis and the Gaussian distribution along the z axis.

where P_1 and P_2 are the powers of the two laser beams. The overlap and the interference can be neglected when $d \geqslant 3w_1$. L denotes the distance between the substrate and the Gaussian center of the first SL. φ represents the phase of the two layers, which is set to be zero for simplicity.

The optical potential associated with the dipole force in low-intensity and large detuning regime is

$$U = \frac{\eta\Delta}{2}\ln\left(1 + \frac{I(x,z)}{I_s}\frac{\Gamma^2}{\Gamma^2 + 4\Delta^2}\right), \qquad (2)$$

where Δ is the detuning, η is Plank's constant divided by 2π, Γ is the natural width of the transition, and $I_{\rm s}$ is atomic saturation intensity. The motion equation of neutral particles in double standing wave light field is given by a set of differential equations[11]

$$\begin{cases} x' = \alpha \\ \alpha' = \frac{1+\alpha^2}{2(E_0-U)}\left(\alpha\dfrac{\partial U}{\partial x} - \dfrac{\partial U}{\partial z}\right) \end{cases}, \qquad (3)$$

where E_0 represents the kinetic energy.

Experimentally the atomic beam scattering from the atom oven is precollimated by an aperture intersecting the atomic beam and further collimated by laser cooling techniques. Generally the longitudinal velocity v_z of the chromium beam obeys the Maxwell-Boltzmann statistics and the initial transverse divergence defined by $\alpha = v_x/v_z$ exhibits a Gaussian spread, where v_x is the transverse velocity. The combined density probability relation between v_z and α can be written as[11]

$$P(v_z,\alpha) \propto v_z^4 \exp\left(-\frac{v^2}{2v_0^2}\left(1+\frac{\alpha^2}{\alpha_0^2}\right)\right), \qquad (4)$$

where v_0 is governed by the oven temperature through

$$0.5mv_0^2 = 0.5k_{\rm B}T_{\rm oven}, \qquad (5)$$

where $k_{\rm B}$ is Boltzmann constant and $T_{\rm oven}$ represents the temperature of the atomic oven. The angle α_0 is given by[17]

$$\alpha_0 = \alpha_{\rm FWHM}/\sqrt[2]{\sqrt{2}-1}, \qquad (6)$$

where $\alpha_{\rm FWHM}$ is obtained through fluorescence experiments. Furthermore, naturally occurring chromium includes approximately 84% ^{52}Cr that is free of hyperfine structure. The other isotopes such as ^{53}Cr and ^{54}Cr do not couple to the laser field. The portion of isotopes is sensitive to experimental geometry during the cooling process[13] . Here we accept the worst case of 16.2%.

Optimized particle optics model[15] where the initial condition is stochastically selected is used to simulate the deposition process in the double Gaussian SLs. The initial condition $(x_i, v_i, \alpha_i, T_i)$ for each trajectory is chosen on a grid with Monte Carlo method. Obviously the initial position x_i is uniformly distributed. The longitudinal velocity v_i and the initial transverse angle α_i just obey the combined probability density relation defined by Eq. (4). T_i determines whether an atom scattering out from the oven is ^{52}Cr or not. If a ^{52}Cr atom comes out, we would resort to differential Eq. (5) to trace the corresponding trajectory; otherwise the trajectory should be a straight line because there is no coupling between the laser field and the atom. At the image plane, a histogram of the probabilities is accumulated as a function of position, resulting in a predicted flux distribution at the surface[11].

The spontaneous emission rate for ^{52}Cr is $\Gamma = 5 \times 2\pi$ MHz and the saturation intensity $I_{\rm s} = 85\,{\rm mW/cm^2}$. The detuning is $\Delta = 250 \times 2\pi$ MHz blue shifted from the resonance. Let $T_{\rm oven} = 1\,823$ K, $\alpha_{\rm FWHM} = 0.16$ mrad, $w_1 = w_2 = 60\,\mu$m, $d = 3w_1$ and $L = 4.2w_1$ respectively. Obviously best focusing process occurs when the two focal planes coincide with the substrate. From the viewpoint of particle optics theorem, the laser power required for bringing the focal plane at the object plane is

given by[11]

$$P_{\text{focus}} = \alpha \frac{\pi E_0 I_s \Delta}{\eta \Gamma^2 k^2}, \quad (7)$$

where α is the excitation parameter. According to Eq. (7), the laser powers that bring the two focal planes at the substrate are $P_1 = 6$ mW and $P_2 = 14$ mW, respectively.

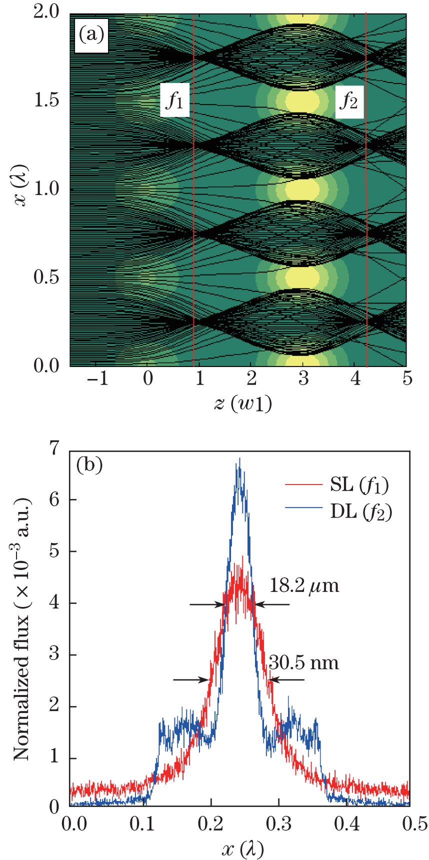

Fig. 4. (a) Trajectory calculation of deposited atoms for four peroids in DL. f_1 is the focal plane of SL, while f_2 is that of DL. In total 200 trajectories are traced; (b) normalized flux distributions at f_1 and f_2, showing feature widths of 30.5 and 18.2 nm, respectively.

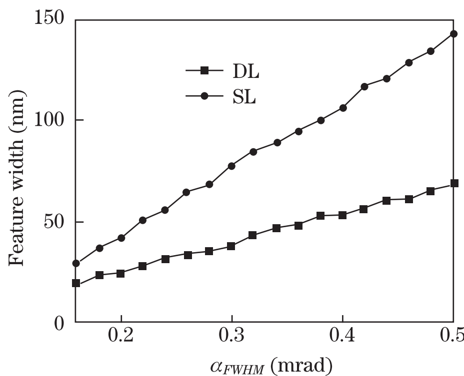

Fig. 5. Feature width as a function of α_{FWHM} for both SL and DL cases.

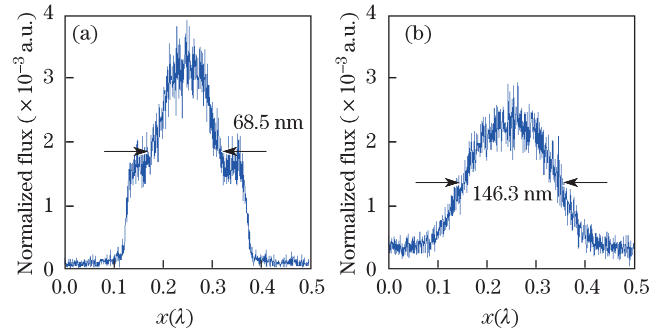

Fig. 6. Normalized flux distributions when α_{FWHM}=0.5 mrad for both (a) DL and (b) SL cases, showing feature widths of 68.5 and 146.3 nm, respectively.

Figure 4 shows the calculated trajectories of atoms in DL and its corresponding feature widths. As can be seen from Fig. 4(a), the spot size of f_2 is much smaller than that of f_1, which we believe arises from the reduction of the spherical aberration. In this configuration, the first layer prefocuses the atoms towards the minima of the sinusoidal potential of the second layer. The light intensity of the second layer $I_2(x,z)$ is proportional to $\sin^2(kx)$ which can be expanded as

$$I_2(x,z) \propto \sin^2(kx) = \frac{1}{2}\left[\frac{(2kx)^2}{2!} - \frac{(4kx)^2}{4!} + \frac{(6kx)^2}{6!} - \cdots\right]. \quad (8)$$

When the prefocused atoms cross the second standing wave, they see closely the parabolic part of the potential which should result in a reduction of the overall spherical aberration. In addition, the feature widths obtained in Fig. 4(b) for both SL and DL cases are 30.5 and 18.2 nm, respectively, when the total amount of the deposited atoms is 5×10^4 in one period. The heights are approximately 8.5 and 12.6 nm for both cases. In comparison with the result with SL shown in Fig. 4(b), a significant reduction of feature width for DL case occurs. Also the height is enhanced considerably. Thus with the prefocusing scheme, a much better deposition result appears, which makes DL a rather competitive candidate for the following experiment.

Since DL mechanism offers a far stronger focusing property than SL, we may expect focusing with relatively large transverse angular distributions. Figure 5 shows the transverse angular dependence of the feature width for both SL and DL cases. The circles represent the trend of SL. The predicted flux is taken from the histogram at f_1 which corresponds to SL. As the angular increases from zero, the feature width shows a rapid increase. When α_{FWHM} is 0.38 mrad, the feature width reaches as large as 100 nm, which is improper for the experiment because the transverse kinetic energy exceeds the depth of the potential well. The squares correspond to the trend of DL. The slope is much smaller that that of SL. As can be seen from Fig. 6(a), well-defined line can still be seen even when α_{FWHM}=0.5 mrad for DL case, with a feature width of 68.5 nm. While in Fig. 6 (b), the feature width for SL reaches as large as 146.3 nm. Thus demand for laser cooling scheme in DL configuration may be reduced considerably.

In Conclusion, latest experimental result with SL is presented in this letter. The feature width obtained is $64 \pm 6n$m and the height of the deposited lines is 4 nm. In order to further reduce the feature width and improve the quality of the focusing process, focusing and depositing characteristics of DL are numerically studied via optimized particle optics model. In comparison with SL, a significant reduction in feature width is predicted even when the transverse angular spread is relatively large. Thus DL is a competitive candidate light mask for the atom lithography experiment.

The project was supported by the National Natural Science Foundation of China (No. 10804084) and the Fundamental Research Funds for the Central Universities (No. 1340-219-042).

References

1. G. Timp, R. E. Behringer, D. M. Tennant, and J. E. Cunningham, Phys. Rev. Lett. **69,** 1636 (1992).
2. J. J. McClelland, R. E. Scholten, E. C. Palmand, and R. J. Celotta, Science **262,** 877 (1993).
3. Y. Ma, T. Li, W. Wu, Y. Xiao, P. Zhang, and W. Gong, Chin. Phys. Lett. **28,** 073202 (2011).
4. F. Lison, H. J. Adams, D. Haubrich, M. Kreis, S. Nowak, and D. Meschede, Appl. Phys. B **65,** 419 (1997).
5. D. Meschede and H. Metcalf, J. Phys. D **36,** 17 (2003).
6. R. W. McGowan, D. M. Giltner, and S. A. Lee, Opt. Lett. **20,** 2535 (1995).
7. R. Ohmukai, S. Urabe, and M. Watanabe, Appl. Phys. B **77,** 415 (2003).
8. E. te Sligte, B. Smeets, K. M. R. van derStam, R. W. Herfst, P. van der Straten, H. C. W. Beijerinck, and K. A. H van Leeuwen, Appl. Phys. Lett. **85,** 4493 (2004).
9. A. Fioretti, A. Camposeo, F.Tantussi, E. Arimondo, S. Gozzini, and C. Gabbanini, Appl. Surf. Sci. **248,** 196 (2005).
10. S. Nowak, T. Pfau, and J. Mlynek, Microelectron. Eng. **35,** 427 (1997).
11. J. J. McClelland, J. Opt. Soc. Am. B **12,** 1761 (1995).
12. W. R. Anderson, C. C. Bradley, J. J. McClelland, and R. J. Celotta, Phys. Rev. A **59,** 2476(1999).
13. E. Jurdik, "Laser manipulation of atomsand nanofabrication", PhD. Thesis (University of Nijmegen, 2001).
14. X. Chen, H. Yao, and X. Chen, Chin. Opt. Lett. **2,** 187 (2004).
15. P. Zhang, Y. Ma, and T. Li, Acta Opt. Sin. **31,** 0514004 (2011).
16. R. Arun, I. Sh. Averbukh, and T. Pfau, Phys. Rev. A **72,** 023417 (2005).
17. R. E. Scholten, R. Gupta, J. J. McClelland, and R. J. Celotta, Phys. Rev. A **55,** 1331 (1997).